PAPER

Check for updates

Experimental and computational approaches to study the chlorination mechanism of pentlandite with ammonium chloride

Xiaolu Xiong, [iD] [a] Guangshi Li,*[a] Zhongya Pang,[a] Sha Chen, [iD] [a] Xingli Zou,[a] Qian Xu,[a] Hongwei Cheng, [iD] [a] Shenggang Li, [iD] [b] Kai Zhu*[a] and Xionggang Lu*[ac]

Pentlandite ($Fe_{4.5}Ni_{4.5}S_8$) is the primary source for the metallurgical production of nickel worldwide, however it usually coexists with copper sulfide in nature. To develop an efficient and green process for the separation and extraction of valuable metals from the nickel sulfide concentrate, herein we conducted experimental studies and density functional theory (DFT) calculations to elucidate the chlorination mechanism of pentlandite using ammonium chloride (NH_4Cl). First, low-temperature chlorination roasting experiments with NH_4Cl were performed in which pentlandite was successfully converted into the corresponding metal chlorides ($FeCl_2$ and $NiCl_2$). Then, the chlorination product was analyzed *via* energy dispersive spectrometry to reveal the elemental distribution at the cross-section. Results reveal that Fe atoms in pentlandite underwent preferential chlorination to form a chloride layer, whereas Ni atoms remained at the center of the grain. Furthermore, density functional theory calculations were performed to investigate the chlorination mechanism of pentlandite by exploring two possible pathways, involving the adsorption of oxygen (O_2), ammonium chloride (NH_4Cl) and chlorine (Cl_2) on both the (001) and (010) surfaces of pentlandite. Considering that the chlorination of pentlandite was achieved in air atmosphere, we first consider the direct chlorination of pentlandite by NH_4Cl in the presence of oxygen. Dissociative oxygen adsorption was found to promote the chlorination process by providing oxygen sites for the dissociation of HCl, which is decomposed from NH_4Cl, eventually leading to the formation of H_2O and $FeCl_2$ species. Alternatively, the reaction between pentlandite and Cl_2 was proved to be feasible thermodynamically.

1. Introduction

Pentlandite, as an important source of nickel, is often used to extract valuable metals for metallurgy. It is usually coexists with copper sulfide in nature and this is called the nickel sulfide concentrate.[1–4] Pyrometallurgical and hydrometallurgical routes have been applied in the industry to extract nickel from the nickel sulfide concentrate.[5] Preactivation roasting–water leaching has proven to be a promising technique for comprehensively recovering valuable metals from the nickel sulfide concentrate.[6–8] Recently, chlorinating roasting, an activated method for chlorinating metals to form metal chlorides, has exhibited high selectivity because of the different thermodynamic stabilities of each metal chloride and has transformed the valuable components of the nickel sulfide concentrate into water-soluble salts.[9–11] Thus, selecting an appropriate chlorinating agent is necessary to achieve the high-efficiency extraction of valuable metals. Conventional chlorinating agents include gaseous chloride (Cl_2 and HCl) and solid chloride.[12–16] Although Cl_2 and HCl exhibit excellent chlorinating performances, the high requirements for equipment and potential hazards restrict their application. Recently, ammonium chloride (NH_4Cl) has shown advantages in extracting valuable metals from raw materials, such as copper and nickel sulfide ores, at a considerably low temperature while remaining active after decomposition.[17–19] NH_4Cl reacts with metal sulfides to produce corresponding metal ammonium chloride salts. When the roasting temperature exceeds 320 °C, these ammonium salts will be further decomposed into the corresponding metal chlorides.[20]

To promote the separation of valuable metals with high efficiency, the chlorination mechanism between the nickel sulfide concentrate and NH_4Cl needs to be investigated. Products obtained from the chlorination process have been extensively investigated using experimental methods, such as X-ray

[a]State Key Laboratory of Advanced Special Steel, Shanghai Key Laboratory of Advances Ferrometallurgy, School of Materials Science and Engineering, Shanghai University, 99 Shangda Road, Shanghai 200444, China. E-mail: lgs@shu.edu.cn; kaizhu@shu.edu.cn; luxg@shu.edu.cn

[b]CAS Key Laboratory of Low-Carbon Conversion Science and Engineering, Shanghai Advanced Research Institute, Chinese Academy of Sciences, 100 Haike Road, Shanghai 201210, China

[c]School of Materials Science, Shanghai Dianji University, 300 Shuihua Road, Shanghai 200240, China

diffraction (XRD), scanning electron microscopy (SEM), and energy-dispersive spectrometry (EDS).[21–24] Rashid *et al.* proposed a technique for iron and copper recovery from copper smelter slag *via* heat treatment with NH_4Cl.[21] Mu *et al.* proposed a novel two-stage chlorination roasting of Ni–Cu matte using an NH_4Cl additive to obtain a high water-leaching rate of nonferrous metals and minimize the formation of the water-soluble Fe salt.[23] Previously, we compared several important features of different chlorination agents, such as their reactivity, economic feasibility and corrosivity, and selected NH_4Cl as an additive while confirming the feasibility of chlorination roasting when using the nickel sulfide concentrate.[25] Generally, the chlorination roasting process has been deemed an efficient technique for separating valuable metals, but few theoretical studies have focused on elucidating the chlorination mechanism.

Density functional theory (DFT) calculations were applied to elucidate the reaction mechanism between gases and solid surfaces at atomic scale.[26,27] Pentlandite being the primary source for nickel extraction, some computational studies have attempted to elucidate the electronic structure of pentlandite. Mkhonto *et al.* modeled the interaction of O_2 with the (110) surface of pentlandite ($Fe_5Ni_4S_8$).[28] They found that the molecular adsorption of O_2 at different surface sites was spontaneous, with the Fe-top site being more favorable over both face-centered-cubic hollow and Ni-top sites. Lu *et al.* studied metal distribution in pentlandite, demonstrating that the metal distribution at tetrahedral sites plays a major role in structural stability.[29] Lu *et al.* further investigated the catalytic activity in hydrogen evolution reaction of pentlandite, involving the (001) and (100) surfaces of pentlandite.[30] Additionally, Anasthasiya *et al.* investigated the interaction between NH_3 and the PbS(100) surface through DFT calculations.[31] The calculated results indicate that the adsorption of NH_3 over PbS is energetically favorable.

We previously studied the oxidation mechanism of complex metal sulfides such as chalcopyrite ($CuFeS_2$) and pentlandite ($Fe_{4.5}Ni_{4.5}S_8$), and elucidated the oxygen migration mechanism and the preferential oxidation of the iron sites using both DFT calculations and experimental studies.[32,33] In a related recent work, we investigated NiS as the intermediate product of Ni_3S_2 oxidation, indicating that O_2 can promote the chlorination of NiS using NH_4Cl and that the generated Cl_2 can promote chlorination process, thus yielding the corresponding metal chloride.[34] This work is aimed at elucidating the chlorination mechanism of pentlandite by NH_4Cl through both theoretical and experimental studies, providing a mechanistic understanding of pentlandite chlorination.

2. Methods

2.1 Experimental methods

The raw materials, obtained from Jinchuan Group Ltd. (China), have been analyzed in our previous work *via* X-ray fluorescence spectrometry (XRF-1800, SHiMADZU LIMITED, Japan).[35] The sample was dried at 100 °C for 24 h and ground into a fine powder (~200 mesh) using an agate mortar. Mineralogical characterization was performed using a tungsten filament

scanning electron microscope, and the elemental distribution was characterized *via* energy-dispersive spectroscopy (EDS) analysis using an SU-1510.

2.2 Computational methods

All calculations were performed using Vienna *ab initio* simulation package (VASP).[36,37] The electrons are completely transferred *via* quantum mechanics through the Kohn–Sham equation. Using the generalized gradient approximation of energy, the energy cutoff value of plane wave expansion is determined to be 400 eV.[38–40] The *k*-point-mesh in the full wedge of Brillouin zone is sampled using a $3 \times 3 \times 1$ grid according to the Monkhorst–Pack grid.[41] Spin-polarized calculations were performed throughout this work. Transition states were calculated using the climbing image nudge elastic band (CI-NEB) method.[42] For each optimized steady state, we calculate the frequency to ensure the accuracy of the transition state. The density of states (DOS) was performed to explain the electronic structure properties of (001) and (010) surfaces of pentlandite. Bader charge analysis were also performed to investigate the electronic properties.[43] The lattice parameters of the bulk of pentlandite obtained herein agree well with those reported in previous literature.[44] The space group of pentlandite is $Fm\overline{3}m$.[44] The (001) and (010) surfaces of pentlandite were considered based on a previous report: minerals mainly cleave along surfaces with large inter-plane spacing during the flotation; these surfaces are usually low-index surfaces with low surface energies. Our slab models for the (001) and (010) surfaces of pentlandite both contain seven atomic layers with a vacuum spacing of 15 Å, thus avoiding interactions between two periodically repeated slabs. The energy of molecules were calculated using a $10 \times 10 \times 10$ Å cubic cell. The bond length of molecular O_2 calculated using our approach is 1.23 Å, which agrees well with the experimental value of 1.21 Å.[45]

3. Results and discussion

3.1 General discussion on the chlorination of pentlandite

Fig. 1 shows a schematic of the chlorination mechanism of pentlandite by NH_4Cl studied both experimentally and *via* DFT calculations. First, the chlorination roasting experiment of pentlandite with NH_4Cl was performed in air atmosphere. Besides, the chlorination of pentlandite involves the chlorination agent (NH_4Cl), atmospheric oxygen (O_2), and possibly the
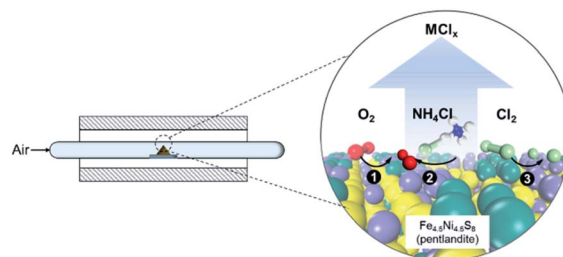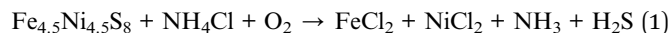

Fig. 1 Schematic of the experimental and DFT studies.

chlorine (Cl_2) formed during chlorination. To reveal the chlorination mechanism of pentlandite through theoretical studies, two possible pathways were considered. In path 1, NH_4Cl reacts with pentlandite directly in the presence of oxygen.

$$Fe_{4.5}Ni_{4.5}S_8 + NH_4Cl + O_2 \rightarrow FeCl_2 + NiCl_2 + NH_3 + H_2S \quad (1)$$

In path 2, the Cl_2 generated during chlorination process reacts with pentlandite.

$$Fe_{4.5}Ni_{4.5}S_8 + Cl_2 + O_2 \rightarrow FeCl_2 + NiCl_2 + SO_2 \quad (2)$$
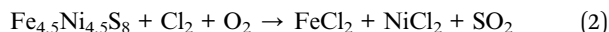
Thus, theoretical work examines the two pathways.

3.2 Elemental distribution during pentlandite chlorination

The chlorination roasting of the nickel sulfide concentrate was achieved using NH_4Cl. As shown in Fig. 2, pentlandite and chlorinate form the main phases in the sulfide concentrates. The Fe_2O_3 phase appeared after a roasting time of 30 min under air atmosphere at 300 °C, which can be attributed to the preferential oxidation of Fe from pentlandite. The detailed reaction mechanism has been discussed in our previous work.[33] The appearance of the NH_4FeCl_3 phase can be attributed to the reaction between the Fe-based sulfides and NH_4Cl.

Fig. 3 shows the EDS-mapping results for Fe, Ni, O, Cl and S elements of the cross-section of a pentlandite particle after chlorination with NH_4Cl at 300 °C. Fe and Cl were mainly found in the shell of the sample with Ni and S located in the core region. This suggests that Fe atoms in pentlandite were preferentially chloridized to form a chloride layer. Hence, combing the XRD and EDS results of the chloridized pentlandite grains reveals that the Fe species were chloridized to iron chloride before the chlorination of the Ni species.

3.3 Chlorination mechanism of pentlandite with NH_4Cl

Early experimental studies show that the chlorination of pentlandite by NH_4Cl can only be achieved in the presence of molecular oxygen. Our calculations show that molecular NH_3 arising from the sublimation of NH_4Cl does not interact with the pentlandite surfaces. Therefore, it was predicted that NH_4Cl would not
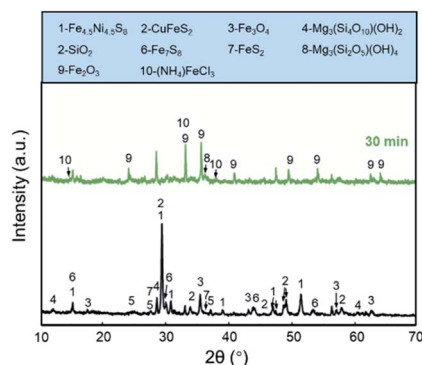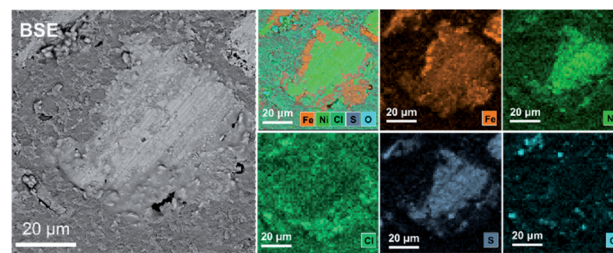

Fig. 3 The EDS-mapping results for elements (Fe−Ni−Cl−S−O, Fe, Ni, Cl, S and O) of a pentlandite particle after chlorination roasting with NH_4Cl at 300 °C in air for 30 min.

directly interact with the pentlandite surfaces in the absence of oxygen. Thus, we considered the possibility of the pentlandite surfaces partial oxidation before its chlorination with NH_4Cl.

3.3.1 The (001) surface. As shown in Fig. 4, oxygen atoms from dissociated O_2 molecules were gradually added to the (001) surface of pentlandite. A monolayer (ML) coverage of adsorbates such as O on the surface is defined by the number of surface metal atoms. Here, the adsorption energy is also defined with respect to molecular O_2: $\frac{1}{2}O_2$ (g) for atomic oxygen adsorption and O_2 (g) for dissociation. The corresponding configurations are presented clearly in Fig. 4(a). Among the adsorption configurations, Fig. 4(i) and (ii) were mentioned in our previous work.[33] In Fig. 4(iii), three oxygen atoms adsorb on the (001) surface with an adsorption energy of −8.79 eV. As there are eight surface metal atoms in the (001) surface of pentlandite, we considered oxygen-covered surfaces with up to four O atoms to attain a coverage of 0.5 ML with an adsorption energy of −11.09 eV (Fig. 4(iv)). In Fig. 4(b), the energies relative to molecular O_2 in the gas phase were predicted to drop with increasing oxygen coverage and to follow a reasonably good linear relationship.

Based on the reaction between molecular O_2 and the (001) surface of pentlandite, we further studied the reaction of pentlandite with NH_4Cl. Fig. 5 shows the potential energy surface and the corresponding adsorption configurations.
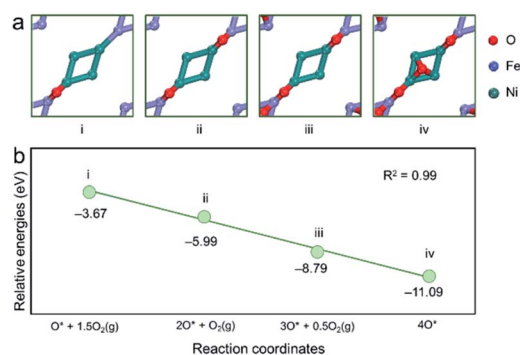

Fig. 4 (a) Top view for atomic oxygen adsorption on the (001) surface of pentlandite at different coverages and (b) correlation between the number of adsorbed O_2 molecules and the adsorption energy (eV) on the (001) surface of pentlandite. ML signifies monolayer, which is defined by the number of surface metal atoms.
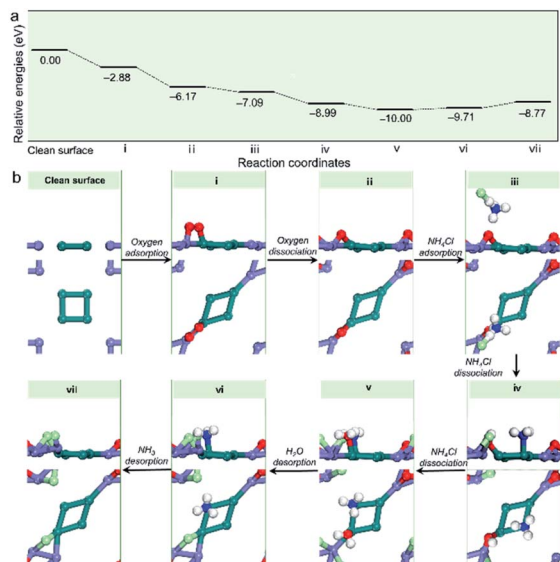

Fig. 2 The XRD patterns for the nickel sulfide concentrate sample and the product obtained with NH_4Cl at 300 °C for 30 min.

Fig. 5 (a) Potential energy profile and (b) corresponding adsorption configurations from side view and top view for NH$_4$Cl adsorption on the (001) surface of pentlandite.

Among the adsorption configurations, Fig. 5(i) and (ii) were calculated in our previous work with molecular oxygen adsorbs on the Ni–Fe bridge site with an adsorption energy of −2.88 eV.[33] Following O$_2$ dissociation, NH$_4$Cl is molecularly adsorbed on the (001) surface with an adsorption energy drop of ∼0.9 eV. Upon dissociation of the NH$_4$Cl molecule on the (001) surface, O–H and Fe–Cl bonds are formed, whereas the NH$_3$ molecule is adsorbed at the Fe top site. H$_2$O is formed with added NH$_4$Cl dissociation with a drop in energy by ∼1.01 eV, indicating that this process is thermodynamically favored. When H$_2$O desorption from the surface, the energy increase for 0.29 eV, indicating that H$_2$O desorption requires energy. After H$_2$O desorption from the surface, a Cl atom can migrate to a neighboring Ni–Fe bridge site, forming an FeCl$_2$ species. Finally, NH$_3$ desorption also requires energy for ∼0.9 eV.

3.3.2 The (010) surface. For the (010) surface, on-surface adsorptions of O$_2$ with coverages of 0.125, 0.25, 0.375 and 0.50 ML were studied. The coverages of 0.125 and 0.25 ML were discussed in our previous work, as shown in Fig. 6(i) and (ii).[33] At 0.75 ML, an added oxygen atom can be adsorbed at the hollow site of Fe–Fe–Ni on the (010) surface, with the adsorption energy dropping to −5.99 eV. When oxygen coverage reaches 0.5 ML, the adsorption energy becomes more negative (−12.46 eV). The average adsorption energy of O$_2$ decreases as the coverage increases from 0.125 to 0.5 ML. A similar trend was reported for oxygen adsorption on Pt and Pd surfaces.[46–48] This indicates that the repulsive interaction between oxygen molecules builds up as coverage increases.

We further studied the interaction between NH$_4$Cl and the (010) surface with adsorbed oxygen atoms. Fig. 7 presents the potential energy surface and the corresponding configurations. Among the configurations, Fig. 7(i) and (ii) were presented in our previous work.[33] NH$_4$Cl molecular adsorption drops by ∼0.9 eV compared with oxygen dissociative adsorption energy
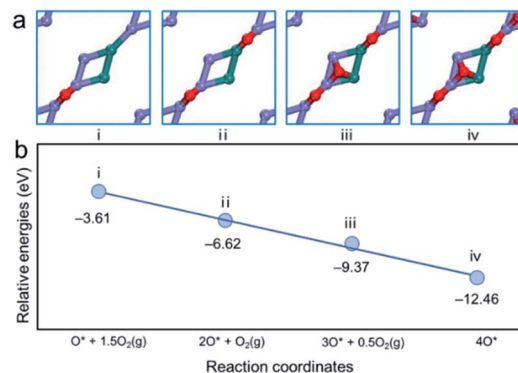

Fig. 6 (a) Top view for atomic oxygen adsorption on the (010) surface of pentlandite at different coverages and (b) correlation between the number of adsorbed O$_2$ molecules and the adsorption energy (eV) on the (010) surface of pentlandite.
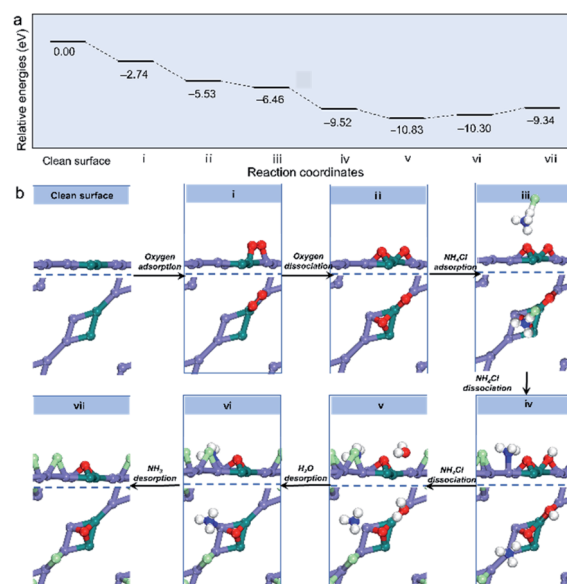

Fig. 7 (a) Potential energy profile and (b) corresponding adsorption configurations for NH$_4$Cl adsorption on the (010) surface of pentlandite from side view and top view.

of −5.53 eV. The dissociation of NH$_4$Cl leads to the adsorption being more negative, by ∼3.0 eV, with the formation of O–H and Fe–Cl bonds. H$_2$O is formed with added NH$_4$Cl dissociation with a drop in energy by ∼1.31 eV, indicating that this process is thermodynamically favored. After H$_2$O desorption from the (010) surface, the relative energy increases by 0.53 eV, indicating that H$_2$O desorption requires energy. NH$_3$ desorption also requires an energy of ∼1.0 eV with the formation of an FeCl$_2$ species. These results demonstrated that NH$_4$Cl chlorination proceeds efficiently on the pentlandite surface when oxygen is preadsorbed in a dissociative manner.

3.4 Chlorination of pentlandite by the generated Cl$_2$

3.4.1 The (001) surface. We first considered the adsorption of a single Cl atom on the (001) surface. As shown in Fig. 8, three
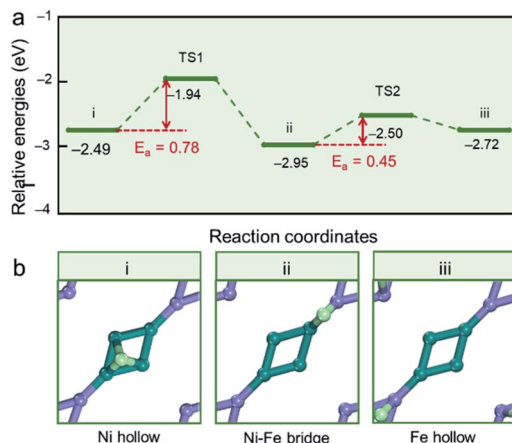
Fig. 8 (a) Potential energy profile and (b) corresponding adsorption configurations for the adsorption and diffusion of single chlorine atom on the (001) surface of pentlandite (top view).

stable adsorption configurations are located: the Ni hollow site, the Ni–Fe bridge site, and the Fe hollow site. The corresponding adsorption energies are −2.49, −2.95, and −2.72 eV, respectively, indicating that atomic chlorine adsorption at the Ni–Fe bridge site produces the most stable configuration, with the chlorine atom interacting with neighboring iron and nickel atoms. In practice, the adsorption configurations for the Cl atoms are similar to those for the O atoms, as both Cl and O atoms are more electronegative than S atoms. Pathway for atomic chlorine migration from the Ni hollow site to the Fe hollow site on the (001) surface is also shown in the figure. The energy barriers were calculated to be 0.78 and 0.45 eV, respectively, suggesting that the adsorbed Cl is easy to diffuse.

Atomic chlorine adsorption energies at different coverages were investigated and the corresponding adsorption configurations were presented in Fig. 9. The adsorption energy decreases by ∼2 eV at a coverage of 0.25 ML. Furthermore, the adsorption energy drops to −8.11 eV because of the strong

interaction between Cl atoms and the surface copper atoms when the coverage reaches 0.375 ML. When Cl coverage reaches 0.5 ML, the adsorption energy becomes more negative (−10.25 eV). A linear correlation was found between the number of adsorbed Cl_2 molecules and the adsorption energy on the (001) surface of pentlandite ($R^2 = 0.99$), indicating that there is almost no interaction between these adsorbates.

3.4.2 The (010) surface. Atomic chlorine adsorption and diffusion on the (010) surface are presented in Fig. 10, where five different adsorption configurations were located. The most stable configuration is the Fe–Fe bridge site, where the chlorine atom interacts with two iron atoms with an adsorption energy of −3.04 eV. The chlorine atom can also adsorbed at the Ni–Fe bridge site with an adsorption energy of −3.02 eV, which approximates the Fe–Fe bridge site adsorption. The adsorption energies for the Fe hollow and Fe–Fe–Ni hollow sites are very similar, although the Fe hollow site is slightly more negative, by 0.01 eV, than the Fe–Fe–Ni hollow site. Thus, the chlorine atom prefers to interact with the iron atom over the nickel atom, leading to more stable adsorption configuration. Furthermore, the energy barriers for chlorine atom migration vary from 0.22 to 0.67 eV, indicating that chlorine atom is mobile on the (010) surface.

As shown in Fig. 11, chlorine atoms from dissociated Cl_2 molecules were gradually added to the (010) surface of pentlandite and the energies relative to molecular Cl_2 in the gas phase were predicted to drop with increasing chlorine coverage. A reasonably good linear relationship is observed between these two quantities. The corresponding configurations are presented in Fig. 11(a). The adsorption energy drops by ∼3 eV at coverage of 0.25 ML. Furthermore, the adsorption energy drops to −8.84 eV because of the strong interaction between Cl atoms and the surface nickel atoms when the coverage reaches 0.375 ML. When Cl coverage reaches 0.50 ML, the adsorption energy becomes more negative (−11.08 eV).

3.5 Electronic structure analysis

To provide further insight into the chlorination mechanism of pentlandite, we performed electronic structure analysis of the pentlandite surfaces. Total and partial DOS analyses of the (001)
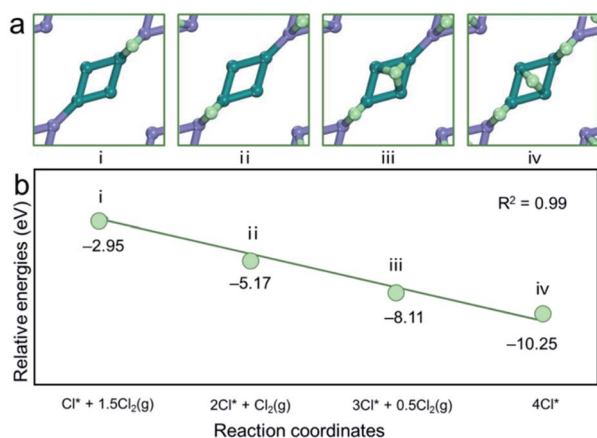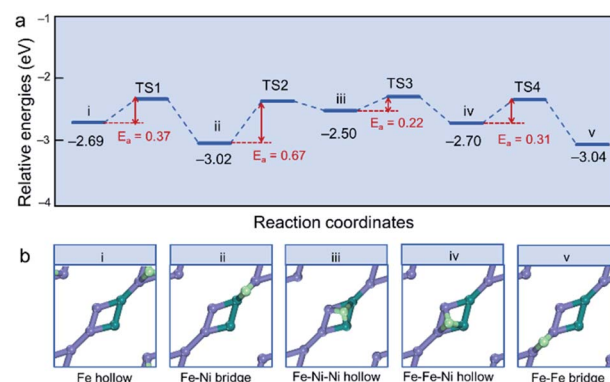

Fig. 9 (a) Top view for atomic chlorine adsorption on the (001) surface of pentlandite at different coverages and (b) correlation between the number of adsorbed Cl_2 molecules and the adsorption energy (eV) on the (001) surface of pentlandite.

Fig. 10 (a) Potential energy profile and (b) corresponding adsorption configurations for the adsorption and diffusion of single chlorine atom on the (010) surface of pentlandite (top view).
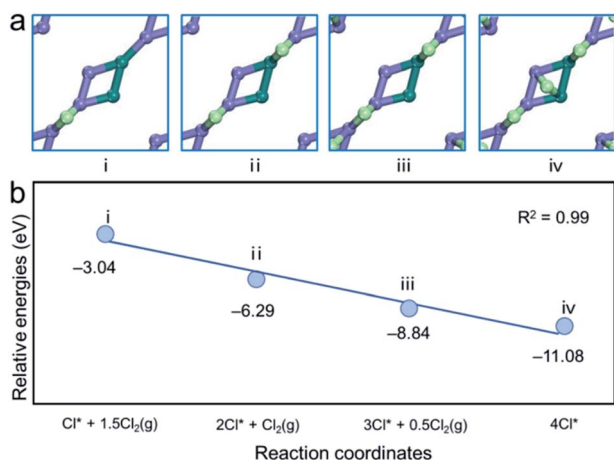
Fig. 11 (a) Atomic chlorine adsorption on the (010) surface of pentlandite at different coverages and (b) correlation between the number of adsorbed Cl_2 molecules and the adsorption energy (eV) on the (010) surface of pentlandite.
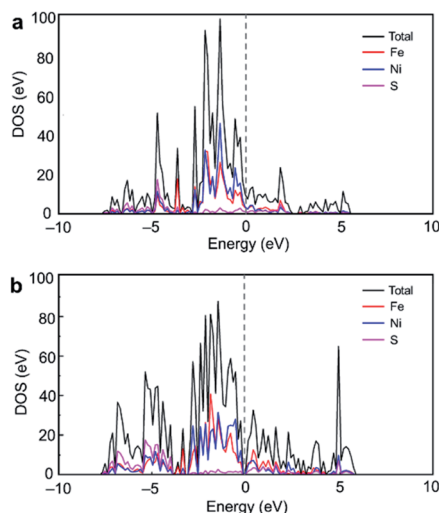

Fig. 12 Total and partial density of states for the (a) (001) and (b) (010) surfaces of pentlandite.

and (010) surfaces are presented in Fig. 12 and no band gap was predicted for both surfaces, suggesting that these surfaces have metallic character.

We further calculated the changes in Bader charges to examine possible electron transfer. As shown in Table 1, Bader charge analysis was performed for atomic chlorine adsorption on the (001) and (010) surfaces. Atomic chlorine was predicted carry more negative charges, suggesting that atomic chlorine serves as electron acceptor, leading to negatively charged. In addition, there is consistency between the amount of transferred charge and the adsorption energy.

3.6 Discussion

An important issue for nickel extraction by chlorination is the separation of nickel chloride from other chlorides. Our EDS

Table 1 Changes in the Bader charges for atomic chlorine adsorption on the (001) and (010) surfaces

Ion Cl	(001)		(010)	
	Configuration	Charge	Configuration	Charge
	Fe hollow	−0.51	Fe hollow	−0.54
	Ni hollow	−0.50	Fe–Ni–Ni hollow	−0.55
	Ni–Fe bridge	−0.56	Fe–Fe–Ni hollow	−0.58
			Fe–Fe bridge	−0.54
			Fe–Ni bridge	−0.58

analysis reveals the distributions of Fe, Ni, O, S, and Cl after chlorination roasting and shows the preferential chlorination of Fe species in the chlorination roasting process. As pentlandite chlorination is a complex process, our calculations focused on the mechanism of the initial reactions of NH_4Cl with the pentlandite surface to understand the preferential chlorination of the Fe species.

Based on our calculation results, the proposed chlorination mechanism of pentlandite with NH_4Cl is shown in Fig. 13. First, oxygen adsorption on the two crystallographic planes of pentlandite was investigated by comparing molecular and dissociative adsorption at different adsorption sites in our previous work and at different surface coverages in this work.[33] The computational results indicate that the interaction between O_2 and pentlandite surfaces is favored thermodynamically and kinetically, revealing the significant role of molecular O_2 during the chlorination roasting of pentlandite with NH_4Cl. The pre-adsorbed oxygen atoms provides suitable sites for the dissociative adsorption of NH_4Cl because of the formation of the considerably stronger O–H bond. This eventually leads to the formation of H_2O on the partially oxidized pentlandite surfaces *via* hydrogen transfer. $FeCl_2$ species is also generated because of the facile migration of Cl atoms.

In addition to the above discussed chlorination mechanism for pentlandite chlorination using NH_4Cl, we investigated another possibility. We assume that molecular chlorine (Cl_2), which was detected in the exhaust gas in some experimental studies, is formed during this process. The calculations for the reaction between Cl_2 and pentlandite surfaces indicate that molecular Cl_2 adsorption on both the (001) and (010) surfaces
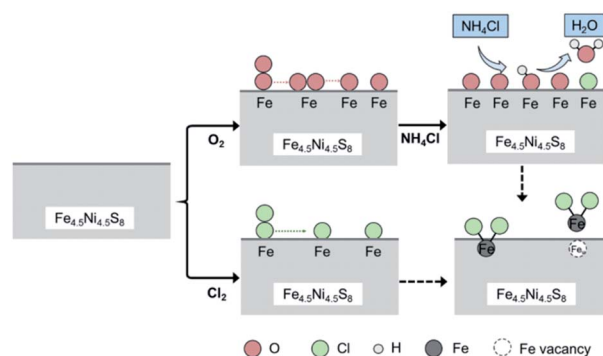

Fig. 13 Schematic chlorination mechanism of pentlandite by NH_4Cl.

can be easily achieved. However, the interaction between Fe atoms of the pentlandite and chlorine is stronger than that of Ni atoms. The top layer of (010) surface contains more Fe atoms, and the adsorption energies are more negative than that of the (001) surface. Bader charge analysis further suggest that there is more charge transferred on the (010) surface. Therefore, the chlorination process of the (010) surface is more favorable than that of the (001) surface. Thus, our computational results are consistent with experimental results, enabling us to provide a mechanistic understanding of pentlandite chlorination.

4. Conclusions

In conclusion, our experimental results show that the Fe atoms migrate to the surface of pentlandite ($Fe_{4.5}Ni_{4.5}S_8$) and are preferentially chloridized, forming the chloride layer. Our periodic DFT calculations on the chlorination of pentlandite reveal that two proposed pathways were feasible. First, the NH_4Cl reacts with the pentlandite surfaces due to the presence of oxygen. The NH_4Cl dissociative adsorption leads to the formation of $FeCl_2$ species. Besides, the reaction between $Fe_{4.5}Ni_{4.5}S_8$ and the generated Cl_2 was favored thermodynamically, indicating that the chlorination can also be achieved by Cl_2 adsorption. Considering the experimental studies and our computational results, two proposed mechanisms can contribute to the chlorination of pentlandite, and our studies provide important insights into the chlorination of pentlandite.

Conflicts of interest

There are no conflicts of interest to declare.

Acknowledgements

Notes and references

1 V. Kirjavainen and K. Heiskanen, *Miner. Eng.*, 2007, **20**, 629–633.

2 S. J. Barnes, S. Staude, M. Le Vaillant, R. Pina and P. C. Lightfoot, *Ore Geol. Rev.*, 2018, **101**, 629–651.

3 D. C. Peck and M. A. E. Huminicki, *Ore Geol. Rev.*, 2016, **72**, 269–298.

4 X. Zeng, M. Xu and J. Li, *Resour., Conserv. Recycl.*, 2018, **139**, 188–193.

5 R. Pandher and T. Utigard, *Metall. Mater. Trans. B*, 2010, **41**, 780–789.

6 W. Mu, F. Cui, Z. Huang, Y. Zhai, Q. Xu and S. Luo, *J. Cleaner Prod.*, 2018, **177**, 371–377.

7 D. Yu, T. A. Utigard and M. Barati, *Metall. Mater. Trans. B*, 2014, **45**, 653–661.

8 G. Zhang, D. Luo, C. Deng, L. Lv, B. Liang and C. Li, *J. Alloys Compd.*, 2018, **742**, 504–511.

9 G. Zhu, R. Chi, W. Shi and Z. Xu, *Miner. Eng.*, 2003, **16**, 671–674.

10 F. J. Alvarez and A. E. Bohe, *Ind. Eng. Chem. Res.*, 2008, **47**, 8184–8191.

11 M. Zhang, G. Zhu, Y. Zhao and X. Feng, *Hydrometallurgy*, 2012, **129**, 140–144.

12 P. V. Aleksandrov, A. S. Medvedev, V. A. Imideev and D. O. Moskovskikh, *Miner. Eng.*, 2019, **134**, 37–53.

13 P. V. Aleksandrov, A. S. Medvedev, V. A. Imideev and D. O. Moskovskikh, *Miner. Eng.*, 2019, **143**, 106029–106035.

14 V. A. Imideev, P. V. Aleksandrov, A. S. Medvedev, O. V. Bazhenova and A. R. Khanapieva, *Metallurgist*, 2014, **58**, 353–359.

15 M. Chakravortty and S. Srikanth, *Thermochim. Acta*, 2000, **362**, 25–35.

16 F. Cui, W. Mu, Y. Zhai and X. Guo, *Sep. Purif. Technol.*, 2020, **239**, 116577–116590.

17 A. N. D'Yachenko and R. I. Kraidenko, *Russ. J. Non-Ferrous Metals*, 2010, **51**, 377–381.

18 A. A. Andreev, A. N. D'Yachenko and R. I. Kraidenko, *Theor. Found. Chem. Eng.*, 2011, **45**, 521–525.

19 P. Wu, L. Zhang, C. Lin, X. Xie, X. Yong, X. Wu, J. Zhou, H. Jia and P. Wei, *Hydrometallurgy*, 2020, **191**, 105225–105235.

20 R. S. Zhu, J. H. Wang and M. C. Lin, *J. Phys. Chem. C*, 2007, **111**, 13831–13838.

21 R. K. Nadirov, L. I. Syzdykova, A. K. Zhussupova and M. T. Usserbaev, *Int. J. Miner. Process.*, 2013, **124**, 145–149.

22 H. Zhu, J. Deng, J. Chen, R. Yu and X. Xing, *J. Mater. Chem. A*, 2014, **2**, 3008–3014.

23 F. Cui, W. Mu, S. Wang, H. Xin, H. Shen, Q. Xu, Y. Zhai and S. Luo, *Sep. Purif. Technol.*, 2018, **195**, 149–162.

24 X. Liu, Y. Feng, H. Li, Z. Yang and Z. Cai, *Int. J. Miner., Metall. Mater.*, 2012, **19**, 377–383.

25 C. Xu, H. Cheng, G. Li, C. Lu, X. Lu, X. Zou and Q. Xu, *Int. J. Miner., Metall. Mater.*, 2017, **24**, 377–385.

26 X. Chen, B. Yang, D. Tao and Y. Dai, *Metall. Mater. Trans. B*, 2010, **41**, 137–145.

27 H. Zhong, L. Wen, C. Zou, S. Zhang and C. Bai, *Metall. Mater. Trans. B*, 2015, **46**, 2288–2295.

28 P. P. Mkhonto, H. R. Chauke and P. E. Ngoepe, *Minerals*, 2015, **5**, 665–678.

29 L. Lu and S. Yu, *Chem. Phys. Lett.*, 2019, **736**, 136786–136793.

30 L. Lu and S. Yu, *J. Colloid Interface Sci.*, 2021, **593**, 116–124.

31 A. N. A. Anasthasiya, G. Kaur, T. V. Beatriceveena, V. Jayaraman and K. I. Gnanasekar, *Appl. Surf. Sci.*, 2019, **495**, 143605–143613.

32 X. Xiong, X. Hua, Y. Zheng, X. Lu, S. Li, H. Cheng and Q. Xu, *Appl. Surf. Sci.*, 2018, **427**, 233–241.

33 X. Xiong, X. Lu, G. Li, H. Cheng, Q. Xu and S. Li, *Phys. Chem. Chem. Phys.*, 2018, **20**, 12791–12798.

34 X. Xiong, G. Li, X. Lu, H. Cheng, Q. Xu and S. Li, *Phys. Chem. Chem. Phys.*, 2020, **22**, 4832–4839.

35 G. Li, X. Zou, H. Cheng, S. Geng, X. Xiong, Q. Xu, Z. Zhou and X. Lu, *Metall. Mater. Trans. B*, 2020, **51**, 2769–2784.

36 G. Kresse and J. Furthmüller, *Comput. Mater. Sci.*, 1996, **6**, 15–50.

37 G. Kresse and J. Furthmüller, *Phys. Rev. B: Condens. Matter Mater. Phys.*, 1996, **54**, 11169–11186.

38 G. Kresse and D. Joubert, *Phys. Rev. B: Condens. Matter Mater. Phys.*, 1999, **59**, 1758–1775.

39 J. Perdew, K. Burke and M. Ernzerhof, *Phys. Rev. Lett.*, 1996, **77**, 3865–3868.

40 P. E. Blochl, *Phys. Rev. B: Condens. Matter Mater. Phys.*, 1994, **50**, 17953–17979.

41 H. J. Monkhorst and J. D. Pack, *Phys. Rev. B: Solid State*, 1976, **13**, 5188–5192.

42 G. Henkelman and H. Jónsson, *J. Chem. Phys.*, 2000, **113**, 9978–9985.

43 W. Tang, E. Sanville and G. Henkelman, *J. Phys.: Condens. Matter*, 2009, **21**, 7.

44 V. T. Rajamani and C. T. Prewitt, *Can. Mineral.*, 1973, **12**, 178–187.

45 *CRC Handbook of Chemistry and Physics*, ed. D. R. Lide, CRC Press/Taylor and Francis, Boca Raton, FL, 2009.

46 Z. Gu and P. B. Balbuena, *J. Phys. Chem. C*, 2008, **112**, 5057–5065.

47 W. Li, C. Stampfl and M. Scheffler, *Phys. Rev. B: Condens. Matter Mater. Phys.*, 2002, **65**, 075407–075426.

48 M. Todorova, K. Reuter and M. Scheffler, *J. Phys. Chem. B*, 2004, **108**, 14477–14483.